Cerebral Bioimaging of Cu, Fe, Zn, and Mn in the MPTP Mouse Model of Parkinson's Disease Using Laser Ablation Inductively Coupled Plasma Mass Spectrometry (LA-ICP-MS)

Andreas Matusch,[b] Candan Depboylu,[c] Christoph Palm,[b] Bei Wu,[a,d] Günter U. Höglinger,[c] Martin K.-H. Schäfer,[e] and J. Sabine Becker[a]

[a] Central Division of Analytical Chemistry, Forschungszentrum Jülich, Jülich, Germany
[b] Institute of Neurosciences and Medicine (INM-1 and −2), Forschungszentrum Jülich, Jülich, Germany
[c] Experimental Neurology, Department of Neurology, Philipps University, Marburg, Germany
[d] Department of Environmental Engineering, Zhejiang University, Hangzhou, China
[e] Department of Molecular Neuroscience, Institute of Anatomy and Cell Biology, Philipps University, Marburg, Germany

Laser ablation inductively coupled plasma mass spectrometry (LA-ICP-MS) has been established as a powerful technique for the determination of metal and nonmetal distributions within biological systems with high sensitivity. An imaging LA-ICP-MS technique for Fe, Cu, Zn, and Mn was developed to produce large series of quantitative element maps in native brain sections of mice subchronically intoxicated with 1-methyl-4-phenyl-1,2,3,6-tetrahydropyridin (MPTP) as a model of Parkinson's disease. Images were calibrated using matrix-matched laboratory standards. A software solution allowing a precise delineation of anatomical structures was implemented. Coronal brain sections were analyzed crossing the striatum and the substantia nigra, respectively. Animals sacrificed 2 h, 7 d, or 28 d after the last MPTP injection and controls were investigated.

We observed significant decreases of Cu concentrations in the periventricular zone and the fascia dentata at 2 h and 7d and a recovery or overcompensation at 28 d, most pronounced in the rostral periventricular zone (+40%). In the cortex Cu decreased slightly to −10%. Fe increased in the interpeduncular nucleus (+40%) but not in the substantia nigra. This pattern is in line with a differential regulation of periventricular and parenchymal Cu, and with the histochemical localization of Fe, and congruent to regions of preferential MPTP binding described in the rodent brain.

The LA-ICP-MS technique yielded valid and statistically robust results in the present study on 39 slices from 19 animals. Our findings underline the value of routine micro-local analytical techniques in the life sciences and affirm a role of Cu availability in Parkinson's disease. (J Am Soc Mass Spectrom 2010, 21, 161–171) © 2010 American Society for Mass Spectrometry

Metal ions are assumed to contribute critically to the pathophysiology and pathogenesis of neurodegenerative diseases such as Parkinson's disease (PD) and Alzheimer's disease [1–4]. Cellular redox imbalance is currently considered to be a major step in the mechanistic cascade leading to cell death [5]. The imbalance consists unanimously in a lower (more negative) cellular redox potential, which is most pronounced in the inner mitochondrial compartment with an increase in the ratio $NADH/NAD^+$. In this scenario, metal cations are protagonists in the active center of almost all redox active enzymes, as components of redox buffer systems, as parts of oxygen transporting globins, and as toxic species like Fe^{2+} and Cu^+ catalyzing radical formation. Mn is known to cause Parkinsonism in primates [6].

A series of studies measured metal concentrations in tissue homogenates of PD brains. With respect to the situation in situ, knowledge has largely been restricted to histochemical stainings of Fe using variations of the Prussian blue reaction [4, 7], labeling free Fe^{2+}/Fe^{3+} and different fractions of bound or precipitated Fe^{2+}/Fe^{3+} depending on the precise experimental conditions, which is a parameter distinct from the total Fe content.

Popescu and coworkers only recently imaged Fe, Cu, and Zn in the midbrain and basal ganglia of a control

Address reprint requests to Dr. J. S. Becker, Central Division of Analytical Chemistry, Forschungszentrum Jülich; 52425 Jülich, Germany. E-mail: s.becker@fz-juelich.de

1044-0305/10/$32.00
doi:10.1016/j.jasms.2009.09.022

Published online October 6, 2009
Received July 13, 2009
Revised September 25, 2009
Accepted September 26, 2009

and a PD case using scanning synchrotron X-ray fluorescence (SRXRF) [8]. Several other studies assessed PD samples using high-resolution techniques with a limited field of view such as high-resolution SRXRF [9, 10]. All these techniques have difficulty in acquiring reliable quantitative data.

In recent years, laser ablation inductively coupled plasma mass spectrometry (LA-ICP-MS) has been developed as the method of choice for the quantitative imaging of elements (especially metals) in biological tissues. LA-ICP-MS imaging of native cryo-sections (optimum at 20–30 μm thickness) has been introduced and developed into a sensitive routine technique in Becker's laboratory at Forschungszentrum Jülich [11–23]. LA-ICP-MS offers a fast and precise spatially resolved measurement of elements in situ at the trace and ultratrace level, including isotope ratios with high analytical throughput and minimal sample preparation at reduced mass spectral interferences. For the quantification of LA-ICP-MS data, strategies using well-prepared homogeneous matrix-matched laboratory standards were established at Forschungszentrum Jülich [11–19, 22–24].

Concerning the choice of samples, it should be noted that the most widely studied neurotoxin animal models for PD are based on local injections of 6-hydroxydopamine (6-OHDA, Scheme **1**) in the nigrostriatal system in rodents, or systemic application of 1-methyl-4-phenyl-1,2,3,6-tetrahydropyridin (MPTP, Scheme **1**) mostly in monkeys or mice.

MPTP was accidentally discovered as a contamination of the illicit opioid meperidine causing a long-lasting Parkinsonian syndrome in humans replicating most features of sporadic PD. The pro-toxin MPTP is oxidized by the monoamine oxidase B (MAO-B), localized within glia to its active metabolite MPP^+, which is then selectively incorporated into dopaminergic neurons via the membrane bound dopamine transporter (Scheme **1**) [25]. As a basic lipophilic compound, it is further enriched within the lipid compartment of the inner mitochondrial membrane where it exerts an effect as a strong and selective inhibitor of Complex I of the respiratory chain. Additional mechanisms of toxicity may be involved. The MPTP model led to a tremendous insight into the mechanisms of neuronal cell death in PD [26, 27]. Recently, Hare et al. [28] presented an approach for measuring in situ metal distributions in three unilaterally 6-OHDA lesioned mice and two sections of one control by LA-ICP-MS.

The aim of the present study was to develop imaging LA-ICP-MS of metals into a routine scale technique and to apply it to a larger statistically representative series of samples. A new software solution allowed the anatomically precise delineation of regions of interest and enabled the kinetics of metal concentrations to be measured after subchronic treatment with MPTP. An additional aim was to employ the established LA-ICP-MS imaging techniques for further understanding of the general metallo-architecture of the mouse brain.

Experimental

The basic workflow of elemental imaging LA-ICP-MS using a quadrupole-based ICP-MS coupled to the laser ablation system (from sample preparation via scanning

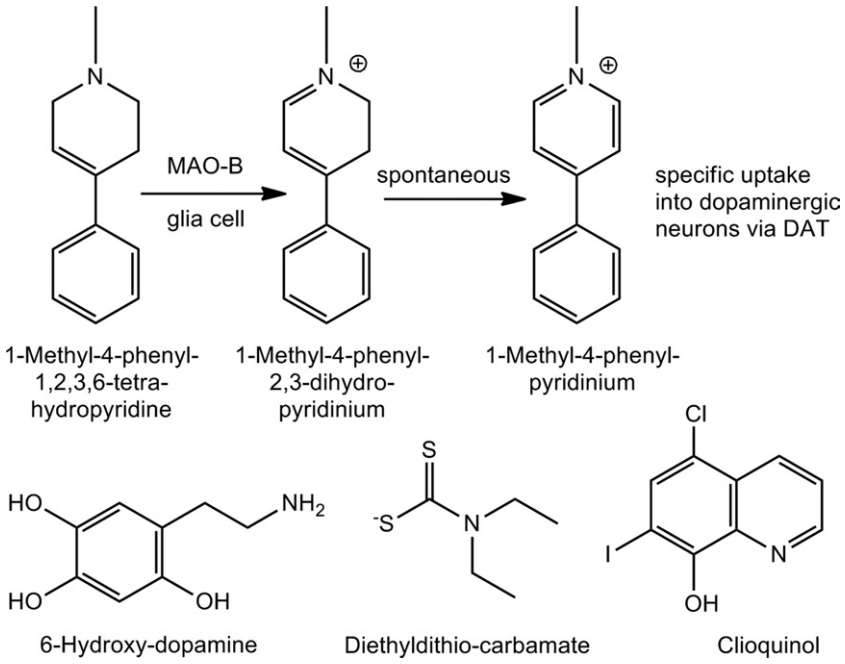

Scheme 1. Structure of the proto-toxin 1-methyl-4-phenyl-1,2,3,6-tetrahydropyridin (MPTP) used in this study, its metabolic activation to MPP+, and structures of the compounds discussed, the neurotoxin 6-hydroxydopamine (6-OHDA), and of the protective copper chelators diethyldithiocarbamate and clioquinol.

of thin tissue slices to the mass spectrometric measurements of ion signals) is illustrated in Figure 1.

LA-ICP-MS Instrumentation

LA-ICP-MS measurements were performed using a quadrupole-based inductively coupled (ICP) mass spectrometer (ICP-QMS, Agilent 7500, Tokyo, Japan) coupled to a laser ablation system (New Wave UP 266, New Wave, Fremont, CA, USA). The material was ablated by a focused Nd:YAG laser and then transported by argon as carrier gas into the inductively coupled plasma (ICP). After ion formation in the ICP ion source, the positively charged ions were extracted from the argon plasma (at ≈100 kPa) via the differentially pumped interface (at ≈130 Pa) between the sampler and skimmer cones into the high vacuum of the quadrupole mass analyzers, and were separated with respect to their mass-to-charge ratios and detected by the ion detector. The experimental parameters of LA-ICP-MS were optimized with respect to the maximum ion intensity of $^{63}Cu^{+}$ using a well-homogenized synthetic laboratory standard. Maximum ion intensity was observed at an rf ICP power of 1500 W and a carrier gas flow rate of 1.2 L min^{-1}. During two-dimensional (2D) imaging of brain tissues, a defined sample area (several cm^2) of a thin section of brain tissue (thickness: 14 μm) was ablated line by line with a focused laser beam. A spot size of the laser beam of 120 μm, a laser power density of 1×10^9 W cm^{-2} and a repetition frequency of 20 Hz were selected. The ion intensities of the analytes, e.g., of $^{64}Zn^{+}$, were measured by LA-ICP-MS line by line at a scan speed of 30 μm s^{-1} in the raster mode throughout the entire ca. 9 mm × 6 mm brain section. All mass spectrometric measurements were performed with established protocols in routine mode in Becker's BrainMet laboratory (BrainMet–Bioimaging of Metals in Brain and Metallomics) at Forschungszentrum Jülich [11–24]. Optimized experimental parameters are summarized in Table 1.

Table 1. Optimized experimental parameters of LA-ICP-MS

ICP-MS	ICP-QMS Agilent 7500 ce
RF power	1500 W
Carrier gas flow rate	1.2 L min^{-1}
Mass resolution m/Δm	300
Laser ablation system	NewWave UP 266
Wavelength of Nd:YAG laser	266 nm
Ablation mode	Scanning (line per line)
Laser pulse duration	20 ns
Repetition frequency	20 Hz
Laser power density	10^9 W cm^{-2}
Number of passes	1
Energy output	50%
Scan speed	30 μm s^{-1}
Laser beam diameter	120 μm
Distance between lines	10 μm

Calibration Procedure

The properties of LA-ICP-MS allow an easy quantification of the measured elements. The distribution profiles of the metals of interest in the brain sections obtained by LA-ICP-MS were quantified using matrix-matched synthetic laboratory standards. Synthetic laboratory standards were prepared from brain homogenates of analogous control mice doped with trace elements of defined concentrations [11, 12]. Milli-Q water or standard solutions with known concentration of analytes

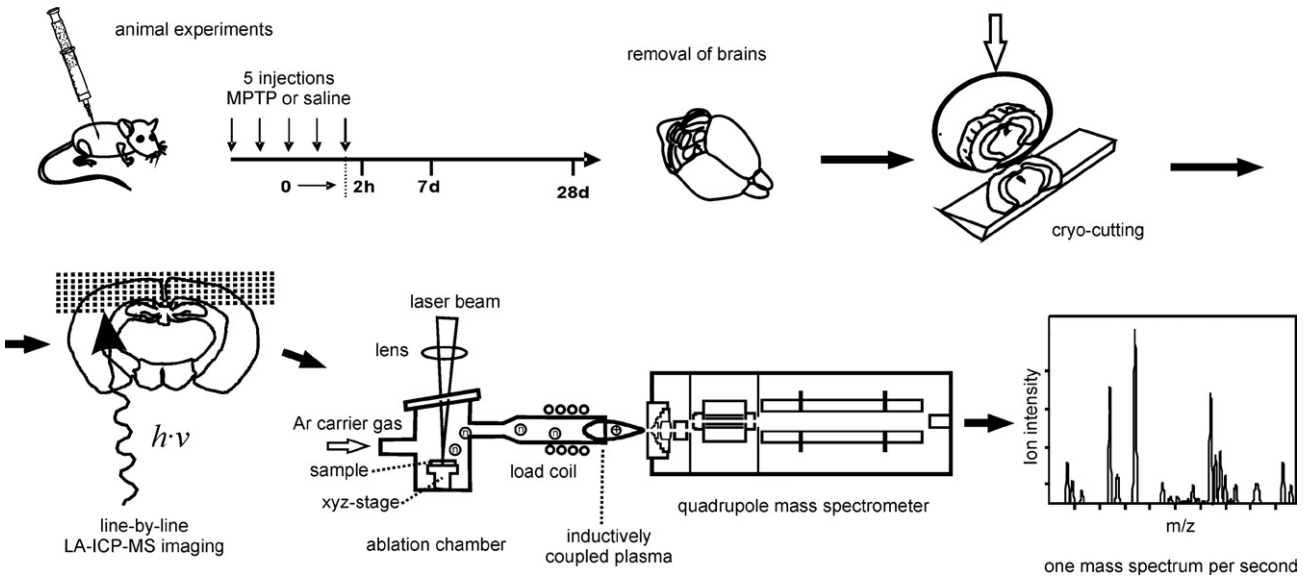

Figure 1. Experimental workflow of the imaging mass spectrometric technique using LA-ICP-MS. MPTP was applied to mice, brains were removed and cryo-cut as scheduled. A thin tissue section was ablated by a focused laser beam in the laser ablation chamber, the ablated material was analyzed mass-spectrometrically, and metal ion images were constructed, quantified, and analyzed regionally.

were added into the brain homogenate. The final added concentrations of metals in the lab standards were 0, 1.2, 2.9, 5.9, 9.2, 12.6, 31, 56, 93, and 110 $\mu g\ g^{-1}$ of 24 elements. The final concentrations of these standards were validated by ICP-MS after microwave-induced digestion with HNO_3 and H_2O_2. These homogeneous lab standards were frozen, cryo-cut into slices, and mounted onto glass slides together with the sample tissue and utilized for the quantification of LA-ICP-MS data in imaging brain tissues in routine mode. Matrix-matched standards were used to constitute calibration curves, whereas the regression coefficient of the calibration curves obtained was typically >0.9 as described previously [12, 15]. To validate the ion images, at least two isotopes, if available, (e.g., $^{63}Cu^+$ and $^{65}Cu^+$ or $^{64}Zn^+$ and $^{66}Zn^+$) were analyzed, and the elemental distribution in neighboring tissue slices was performed under the same experimental parameters. Possible isobaric interferences of single-charged analyte ions with polyatomic ions or double-charged ions were studied carefully and minimized under optimum experimental conditions.

Data Treatment

No commercial software is currently available to evaluate analytical LA-ICP-MS data for the imaging of elements. We developed software packages with the aim of obtaining three-dimensional (3D) metal or non-metal distributions, e.g., in mouse or rat brain, to correlate the data with MRI (magnet resonance images) immunostained, autoradiographic, and histochemical images of the same rat brain at Forschungszentrum Jülich.

The data output from the mass spectrometer was organized in columns of signal values at consecutive time points for every element in a single ASCII file. These lists of measurements were transformed into an image of element count rates to visualize their spatial distribution using a software tool written in-house. The software takes into account parameters such as line length, number of lines, data offset at start and at end, as well as the diameter of the laser beam and the distance between the lines. The pixel size of the resulting images is determined according to the highest common factor of line distance and spot diameter. Values between scanned lines are filled by linear interpolation in the y-direction. The range of values to be displayed in an 8-bit graphic was chosen from the lowest pixel value to the highest biological value, disregarding data artifacts out of the sample area. The reconstructed element image was exported as 8-bit grayscale TIFF file and optionally as a color image after pseudo-coloring with a rainbow color map. Further treatment of the images in terms of calibration and region-of-interest (ROI) selection was done with Pmod version 2.95 (Pmod, Zürich, Switzerland).

Precise anatomical ROIs were delineated according to the corresponding plane from the Paxinos' and Franklin mouse brain atlas [29] integrating the topographical information from Zn, Cu, Fe, Mn, C, and P maps and from adjacent sections stained with cresyl violet. The entire brain area was covered by regions. The average signal was computed in each freely drawn region. Finally, the raw images were scaled after subtraction of the averaged glass offset, thus yielding parametric images of element concentrations. The linearity of the data conversion was verified.

Absolute calibrations were available for 14 of the 39 sections. In the remaining images, the signal was normalized to the average of a reference region. The reference region was the corpus callosum for most elements. In Cu images, the corpus callosum was outshined too much by the extremely high Cu signal of the adjacent sub- and periventricular zone, therefore, cortex layer II and III proved as better reference regions. In some Fe images, the upper third of an image, including the corpus callosum, showed a signal drift. Therefore, a reference region at the same vertical height as the most interesting SN and with comparatively low Fe signal was chosen, including ventral neo- and archicortical areas. The background signal, averaged from the blank glass surrounding was subtracted from each regional signal.

A univariate one-way analysis of variance (ANOVA) was used to compare the means of regional element concentrations between the groups control, 2 h, 7 d, and 28 d post-MPTP. P values as the level of significance indicate the probability that within-group variances equal between-group variances. Upon the a-priori hypothesis that kinetics after the intervention are an increase, a decrease, or follow a u-shape, corresponding contrasts were tested. A $P < 0.05$ was considered as significant. The SPSS version 17.0 software (SPSS Inc., Chicago, IL, USA) was used for statistics.

Animal Experiment and Sample Preparation

All animal experiments were approved by the local authorities (Regierungspräsidium Gießen) and were performed in accordance with current guidelines. Wild-type C57Bl6 male mice, 8 to 10 wk old, were injected with 30 mg kg^{-1} MPTP (3 mg mL^{-1} saline) or vehicle intra-peritoneally on 5 consecutive d according to [27, 30]. Animals were sacrificed 2 h, 7 d, or 28 d after the last injection using 100 mg kg^{-1} pentobarbital and immediately perfused with saline. Time points were chosen to best represent the pathologic stages of ongoing degeneration (2 h), maximal degeneration (7 d), stable lesion and astrogliosis (28 d). Brains were removed and frozen in isopentane at −78.5 °C. Cryosections of brains and standards of 14 μm thickness were mounted on silanized slides. Neighboring sections were stained with cresyl violet.

Characterization of the MPTP Model

Dopamine within striatal fragments dissected from animals treated in parallel within the same experiment was quantified by high-pressure liquid chromatography (HPLC) with electrochemical detection. Briefly, the

tissue was homogenized in 500 μL perchloric acid (0.4 N) for 1 min. After centrifugation at 13,000 *g* and 4 °C, the supernatants were passed through a 0.2 μm filter; 20 μL aliquots were injected by an autosampler cooled at 4 °C on a Knaur Nucleosil 120 Å C18 column (250 × 4 mm, precolumn 5 × 4 mm; Knaur, Berlin, Germany) maintained at 45 °C by a column oven. Isocratic elution at 0.5 mL min^{-1} used acetonitrile/water 3.5/97.5 containing 0.6% triethanolamine adjusted to pH 2.95 with phosphoric acid 100 mg L^{-1} Na_2EDTA and 140 mg L^{-1} octane-sulfonic acid. The detector potential of a glassy carbon electrode was set to 750 mV against an Ag/AgCl reference electrode. Chromatograms were recorded and analyzed by the HPLC computer system Chromeleon (Dionex, Germany).

Immunohistochemistry was carried out on free-floating paraformaldehyde-fixed and sucrose-protected brain cryo-sections with a polyclonal antibody against tyrosine hydroxylase (TH; Chemicon, Germany), using standard avidin-biotin-peroxidase techniques (Vectastain Elite ABC kit; Boehringer, Germany) and visualized enzymatically by incubation with 3,3′-diaminobenzidine (DAB; Sigma-Aldrich, St. Louis, MO, USA), enhanced by the addition of nickel ammonium sulfate (Fluka, Buchs, Switzerland), resulting in a dark blue staining [31]. The number of TH+ neurons within the substantia nigra was determined on several sections per animal.

Results and Discussion

New Achievements in LA-ICP-MS Imaging Techniques

The reproducibility of the imaging LA-ICP-MS technique for the analysis of 20 μm thin cross sections of biological tissues was studied by Becker and coworkers [21]. A reproducibility of about 3% had been observed for homogeneous tissues (e.g., thin sections of matrix-matched laboratory standards) and a reproducibility in the range of 5%–7% for inhomogeneous tissues (adjacent sections of inhomogeneous human brain) comparing the distribution of the elements of interest. In the present study, replicate measurements of two or three adjacent sections were highly reproducible with coefficients of variation of 5% for Fe and Cu, 12% for Zn, and 11% for Mn in the striatum.

In the present study, quantitative images of metals were obtained in brain slices from mice in a time course series after intoxication with MPTP. Sections at an anterior level crossed the striatum and those at a posterior level crossed the hippocampus and the substantia nigra, thus covering the most relevant structures for PD research. The subchronic MPTP intoxication paradigm induced a homogeneous and reproducible degeneration of the nigrostriatal dopaminergic neuronal projection as indicated by a considerable and partially reversible decrease in nerve fibers in the striatum (Figure 2a) and in striatal dopamine levels (Table 2) compared with saline-treated controls. The number of TH immunostained neurons in the substantia nigra decreased irreversibly (Figure 2b, Table 3). TH is the key enzyme of the dopamine biosynthesis and the most widely used marker for dopaminergic neurons and terminals that are selectively hit by MPTP.

We implemented in-house software to reveal the spatial distribution of LA-ICP-MS data followed by a comprehensive data analysis utilizing atlas-related free-form ROIs, calibration, and statistical analysis by commercially available image analysis and statistics soft-

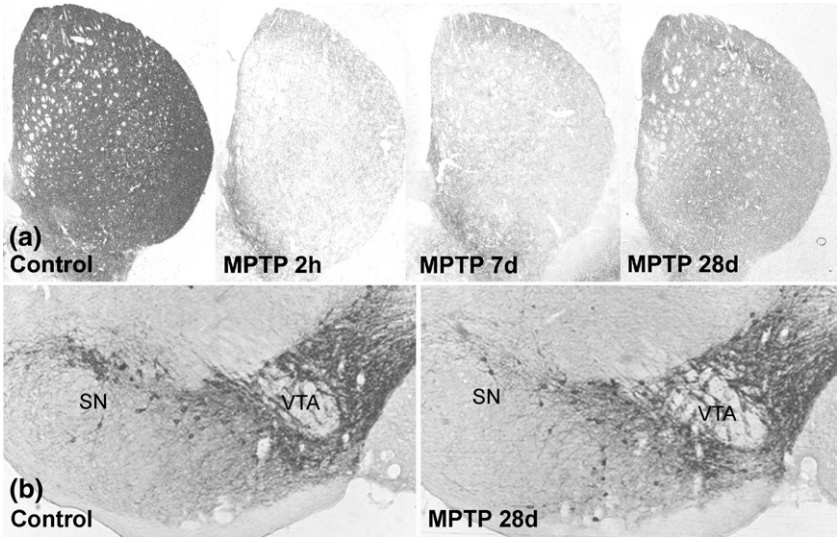

Figure 2. Nigrostriatal dopaminergic pathway injury induced by subchronic MPTP treatment was characterized by antibody staining for tyrosine hydroxylase (TH), the key enzyme of dopamine biosynthesis and a marker of dopaminergic neurons and fibers. (**a**) A considerable early decrease and later a partial recovery of dopaminergic fibers occurred in the striatum. (**b**) An irreversible loss of dopaminergic neurons occurred in the substantia nigra. Shown are photomicrographs of coronal sections.

Table 2. Concentrations of Fe, Cu, Zn, Mn measured by imaging LA-ICP-MS in selected regions of interest characteristic of each element in the brain of mice (18 animals) at different time points after MPTP treatment versus controls. For comparison measures characterizing the lesion to the dopaminergic system are given: the total count of cells positive for tyrosine hydroxylase immunostaining (TH+) within the substantia nigra reflecting the irreversible lesion to cell bodies and dopamine concentrations measured by HPLC of extracts from striatal tissue reflecting the partially reversible lesion to neuronal terminals

					ANOVA	
μg g^{-1} wet weight	Control	MPTP 2 h	MPTP 7 d	MPTP 28 d	*P** global	*P*** increase
Fe						
Interpeduncular	4.5 ± 0.7	5.3 ± 1.0	6.2 ± 0.8	6.2 ± 1.5	-	0.025
Cu						
Periventricular	8.9 ± 2.2	7.0 ± 1.0	7.9 ± 1.1	12.3 ± 4.2	0.008	-
Aquaeduct	5.0 ± 1.2	4.2 ± 0.2	5.9 ± 1.9	5.8 ± 2.4	-	-
Ventral FD	4.6 ± 0.8	3.3 ± 0.6	5.2 ± 1.0	4.5 ± 1.0	0.001	0.005
Dorsal FD	2.2 ± 0.3	1.9 ± 0.2	2.4 ± 0.4	2.2 ± 0.5	0.031	0.07
Presubiculum	2.6 ± 0.4	2.2 ± 0.2	2.6 ± 0.4	2.3 ± 0.5	-	-
Zn						
CA3/PolDG	25.6 ± 3.9	22.3 ± 1.9	25.3 ± 2.1	27.0 ± 4.8	0.038	0.07
Dorsal FD	9.5 ± 1.7	8.9 ± 1.0	9.3 ± 1.4	9.3 ± 0.9	-	-
Piriform CTX	8.3 ± 0.8	9.4 ± 1.2	8.6 ± 1.4	9.3 ± 1.5	-	-
Mn						
Ncl. Ruber	0.36 ± 0.05	0.32 ± 0.02	0.35 ± 0.01	0.36 ± 0.09	-	-
Nigral TH+-cell count	9459 ± 537	6293 ± 466	5227 ± 319	5148 ± 600	<0.001	***
Striatal Dopamine concentration μg g^{-1}	22.5 ± 2.9	5.4 ± 0.7	7.8 ± 0.7	14.3 ± 2.2	<0.001	****

Data are given as mean ± standard deviation.
- = not significant; ANOVA = analysis of variance; CTX = cortex; FD = fascia dentata; Ncl = nucleus; PolDG = polymorph layer of the dentate gyrus; TH+ = positive for tyrosine hydroxylase immunostaining.
*A univariate one-way analysis of variance was used to compare group means. *P* values as level of significance indicate the probability that within-group variances equal between-group variances. $P < 0.05$ was considered as significant.
**Level of significance yielded from the contrast (−1, −1, 1, 1) assuming a two-step increase in the order Ctrl = 2h < 7d = 28 d.
***The *P* value for nigral cell counts was $P = 0.00000009$ resulting from global ANOVA. Post hoc Bonferroni tests for multiple comparisons yielded significantly ($P < 0.000006$) higher values in the control group compared to all other groups and in addition significantly higher values at 2 h compared with 28 d ($P = 0.04$).
****The *P* value for striatal dopamine concentrations from parallel animals was $P = 0.00000010$. Post hoc Bonferroni tests for multiple comparisons yielded significantly ($P < 0.0004$) higher values in the control group compared wit all other groups. In addition, partially recovered dopamine concentrations at 28 d significantly exceeded values at 2 h and 7 d ($P < 0.002$).

ware. A set of anatomical ROIs was freely delineated for each section based upon the topographic information provided by images of Zn, Cu, Fe, Mn, C, and P by cresyl-violet-stained adjacent sections in conjunction with the corresponding plane of the mouse brain atlas [29].

LA-ICP-MS imaging yielded a highly reproducible architecture of element distributions in line with previous findings by others and ourselves [7, 13, 28]. On the basis of maps of Fe, Zn, Cu, Mn, C, and P, it was possible to define a consistent set of ROIs precisely matching the topography revealed by cresyl-violet stains (Figure 3).

Metallo-Architecture in the Normal Mouse Brain

Examples of element maps of coronal sections at an anterior plane and a posterior plane are shown in Figures 4 and 5 for each condition. The location of the highest Fe concentration was the interpeduncular nucleus followed by the dorsal and ventral pallidum. This was in line with modified Prussian blue stainings of rat brains [7]. Cortical Fe was concentrated in the outer and inner granular layer (II and IV), whereas Fe was low in the inner pyramidal layer V and the multiform layer (IV). The Cu concentration was highest in the periventricular zones, exceeding the cortex and basal ganglia by a factor of 5. Other regions of elevated Cu concentrations were the ventral (factor 3) and dorsal fascia dentata (granular layer), the supramamillar nucleus and the presubiculum (factor 1.5). Cu allowed a clear delineation of the cornu ammonis, the striatum and cortical layers.

Zn was clearly most concentrated in the portion of CA3 belonging to the dentate gyrus (polymorph layer) followed by the rest of CA3, the amygdala, the piriform cortex, and cortical layer I. In comparison, Zn concentrations were extremely low in other areas.

High Mn was observed in the medial hypothalamus, in the nucleus ruber, in the accessory oculomotor nucleus, and, to a lesser extent, in the substantia nigra.

Mg was almost homogenously distributed with slight systematic enrichments in areas of high cell density, such as the fascia dentata or distinct cortical layers, and in white matter. Na and K showed a homogeneous distribution (data not shown).

As in our previous studies C, P, and S showed slight but consistent elevations in white matter corresponding to the lower water content of 70% compared with 80% in gray matter. In addition, for sulfur a modest enrichment in striatum was found.

Table 3. Concentrations of Fe, Cu, Zn, Mn (mean ± SD) measured by imaging LA-ICP-MS in "large" regions of interest in the brain of mice (18 animals) at different time points after MPTP treatment versus controls

$\mu g\ g^{-1}$ wet weight	Control	MPTP 2 h	MPTP 28 d	MPTP 7 d	ANOVA		
					*P** global	*P*** increase	*P**** U-shape
Striatum							
Fe	3.7 ± 0.5	3.6 ± 0.2	4.2 ± 0.4	3.9 ± 0.3	-	0.018	-
Cu	1.6 ± 0.1	1.7 ± 0.2	1.7 ± 0.1	1.7 ± 0.2	-	-	-
Zn	7.3 ± 0.5	8.4 ± 0.8	7.7 ± 0.5	8.1 ± 1.1	-	-	-
Mn	0.16 ± 0.04	0.18 ± 0.00	0.17 ± 0.03	0.18 ± 0.01	-	-	-
S. Nigra							
Fe	4.2 ± 0.7	3.8 ± 0.3	3.9 ± 0.2	4.4 ± 0.2	0.018	-	0.003
Cu	1.7 ± 0.3	1.4 ± 0.1	1.6 ± 0.2	1.6 ± 0.3	-	-	-
Zn	6.6 ± 1.5	5.8 ± 0.3	6.3 ± 0.6	6.3 ± 0.8	-	-	0.08
Mn	0.30 ± 0.05	0.20 ± 0.04	0.27 ± 0.01	0.30 ± 0.04	0.019	-	0.012
Cortex							
Fe	3.5 ± 0.2	3.7 ± 0.3	3.5 ± 0.3	3.7 ± 0.3	-	-	-
Cu	1.7 ± 0.2	1.6 ± 0.1	1.7 ± 0.2	1.5 ± 0.2	0.029	0.015****	-
Zn	8.3 ± 1.3	8.2 ± 0.7	8.2 ± 0.8	8.0 ± 1.1	-	-	-
Mn	0.20 ± 0.03	0.20 ± 0.03	0.19 ± 0.04	0.18 ± 0.03	-	-	-
VP-laHT							
Fe	4.3 ± 0.6	4.6 ± 0.4	4.9 ± 0.2	4.7 ± 0.7	-	-	-
Cu	1.2 ± 0.1	1.2 ± 0.2	1.7 ± 0.5	1.4 ± 0.3	0.045	0.014	-
Zn	6.6 ± 0.5	7.6 ± 0.8	8.2 ± 1.4	8.0 ± 1.7	0.06	0.025	-
Mn	0.26 ± 0.10	0.26 ± 0.03	0.31 ± 0.05	0.31 ± 0.02	-	-	-

Data are given as mean ± standard deviation.
- = not significant; ANOVA = analysis of variance; VP-laHT = ventral pallidum and lateral hypothalamus.
* A univariate one-way analysis of variance (ANOVA) was used to compare group means. *P*-values as level of significance indicate the probability that within-group variances equal between-group variances. $P < 0.05$ was considered as significant.
** Level of significance yielded from the contrast (−1, −1, 1, 1) assuming a two-step increase in the order Ctrl = 2 h < 7 d = 28 d.
*** Level of significance yielded from the contrast (1, −1, −1, 1) assuming U-shaped kinetics in the order Ctrl > 2 h = 7 d < 28 d.
**** Level of significance yielded from the contrast (1.5, 0.5, −0.5, −1.5) assuming a continuous decrease in the order Ctrl > 2 h > 7 d > 28 d.

Changes Following MPTP Intoxication

Average concentrations of Fe, Cu, Zn, and Mn throughout different regions in control animals and in animals sacrificed at different time points after MPTP are given in Tables 2 and 3 in parallel with the time course of the dopaminergic lesion (Table 3). Significant results from one-way ANOVA are indicated. Figures 4 and 5 illustrate findings by quantitative element maps from a representative section of each group.

The highest change observed was a 38% increase versus the control of Cu at 28 d following a roughly 10% decrease at 2 h and 7 d in the periventricular zone. In the fascia dentata, a significant initial 17% and 27% (dorsal and ventral) decrease at 2 h was followed by a compensatory increase to control level at d 7 and 28. The common motif of these asynchronous kinetics was a decrease followed by a compensation or overcompensation. In contrast, cortical Cu significantly decreased by 10% not earlier than at 28 d.

Fe significantly and continuously increased by 38% and 39% at 7 and 28 d, respectively, in the interpeduncular nucleus. Comparatively slight changes of Fe were found in the substantia nigra suggesting a u-shaped kinetics with a roughly 10% decrease at 2 h and 7 d and compensation to normal levels at 28 d. Zn and Mn concentrations were equal to control levels at the late time point following slight initial decreases in the polymorph layer of the dentate gyrus. No changes were observed in C, P, and S.

Correlation with Previous Findings

The slight changes of element concentrations observed, not exceeding 40% compared with controls, were in line with the mild nature of the subchronic MPTP model chosen to mimic the slow course of the human disease. Especially in the PD-related candidate regions, substantia nigra and striatum element concentrations were almost constant.

Rios and coworkers [32] studied the identical MPTP model (5 injections of 30 mg kg^{-1}) at d 7 as a single time point, dissected the mouse brains into four large parts and analyzed Cu, Mn, and Pb in digests by atomic absorption spectroscopy (AAS). We were able to reproduce the tendency to a Cu decrease in the striatum but not to the extent of 50% (only 10% here). In the cortex, as in our study, all element concentrations were constant in a margin of ±10%. Mn showed a 20% versus 7% decrease in the striatum and, similar to this study, constancy in the cortex and mesencephalon.

Clearly, considerable changes in small regions such as the periventricular zone are diluted within these large fragments. Measurements vary to a great extent with respect to whether this small zone at the margin with major Cu contribution is included into the striatal tissue block or not.

Recently, Salazar and coworkers [33] studied the time course of ventrolateral mesencephalic Fe measured

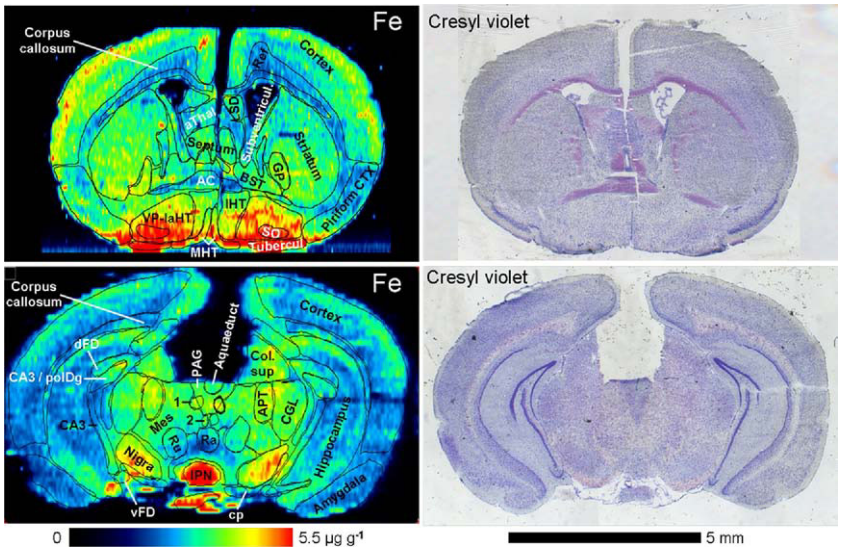

Figure 3. Sets of individually delineated regions of interest in coronal mouse brain sections as used in the anterior series (upper row) and the posterior series (lower row) are exemplified in LA-ICP-MS concentration maps of Fe (left). Microphotographs of cresyl-violet-stained adjacent sections permit anatomical correlation (right). Upper row: AC = anterior commissure; aThal = anterior thalamic region; BST = bed nucleus of the stria terminalis and stria terminalis; Ref. = reference region for Fe composed of corpus callosum and the adjacent cortical layers V and VI; GP = globus pallidus; IHT, intermediate hypothalamus; LSD = lateral septal nucleus, dorsal part; MHT = medial hypothalamus; piriform CTX = piriform cortex; SO = nucleus supraopticus; subventricul. = periventricular zone as defined by Cu enrichment; tubercul. = tuberculum olfactivum; VP-laHT = ventral pallidum-lateral hypothalamus. Lower row: 1 = nucleus interstitialis Cajal; 2 = nucleus oculomotorius accessorius; APT = anterior pretectal nucleus; CA3 = part 3 of the cornu ammonis, ventral portion; CA3/polDG = dorsal portion of CA3 equaling the polymorph layer of the gyrus dentatus; CGL = corpus geniculatum laterale; Coll. Sup. = colliculus superior; cp = cerebral peduncle; dFD = dorsal fascia dentate; IPN = interpeduncular nucleus; Mes = mesencephalon, not classified otherwise; Nigra = substantia nigra; PAG = periaqueductal gray; Ra. = nucleus Raphé; Ru. = nucleus rubber; vFD = ventral fascia dentata.

by AAS in dissected tissue after acute MPTP. After a maximum increase of 29% at d 2, they observed an 18% decrease at d 7 and a 10% increase at d 21.

Fe concentrations of 5–6 μg g^{-1} wet weight in controls were very close to the value of $\approx$4 μg g^{-1} observed in this study.

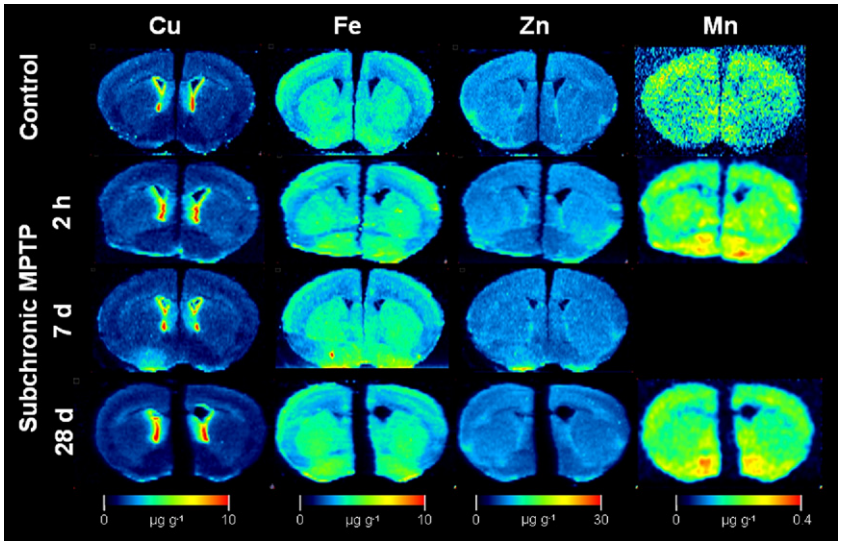

Figure 4. Quantitative metal images of Cu, Zn, Fe, Mn representative of each group (control, 2 h, 7 d, and 28 d after the last of five daily MPTP injections). Sections on an anterior level crossing the lateral ventricles, the striatum and the hypothalamus. Note the increase of copper in the periventricular region at 28 d of MPTP.

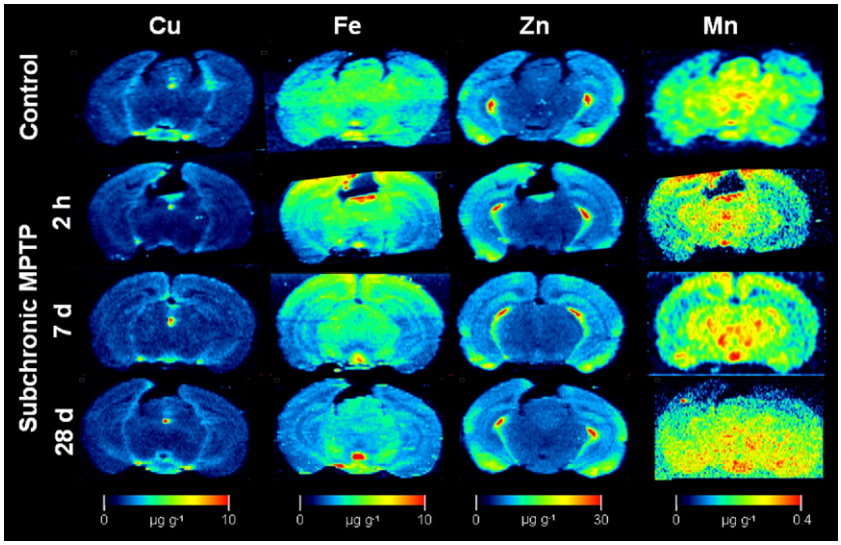

Figure 5. Quantitative metal images of Cu, Zn, Fe, Mn representative of each group (control, 2 h, 7 d, and 28 d after the last of five daily MPTP injections). Sections on a posterior level crossing the substantia nigra, the interpeduncular nucleus and the hippocampus. Note the increase of copper in the aqueduct and of iron in the interpeduncular nucleus at 7 d and 28 d of MPTP.

Sections from contralateral hemispheres were processed with modified Prussian blue staining, but only small details of these sections were shown, not covering the interpeduncular nucleus. Only mild nigral staining was described in controls with a restricted localized increase at 2 d MPTP. Another study assessed Prussian blue positive cells in controls, 3 and 7 d after acute MPTP (3×30 mg kg^{-1}), which covered 0.3%, 0.4%, and 0.6% of the nigral area respectively [34]. Apparently, this small fraction would not significantly influence total nigral Fe content.

Our findings in the subchronic MPTP mouse model clearly differ from findings in the more aggressive 6-OHDA rat model, where tremendous increases of Fe, Cu, Zn, and Mn in the basal ganglia were measured by ICP-MS on dissected tissue fragments [35].

Mechanistic Interpretation

Amongst our findings was an initial decrease of Cu, reversible in the fascia dentata and with a 40% rebound in periventricular zones. This could simply result from an overlay of regions with high Cu content and regions with high susceptibility to MPTP (vide infra). The direction of this effect remains to be explained, as well as the concomitant slight but significant continuous decrease of Cu in the cortex and brainstem. Therefore, it must be remembered that on a cellular level, Cu is first passively taken up by the selective copper transporter Ctr1 [36, 37] and then actively sequestered by the ATP-consuming copper efflux pumps ATP1A [37] and ATP1B [38]. Thus, the transport of Cu across cellular barriers such as the blood-brain (BBB) and the blood cerebrospinal fluid (CSF) barrier (BCB) consumes energy. MPTP causes a severe breakdown of the cellular energy metabolism with a depletion of ATP. It therefore seems plausible that coinciding with the maximal toxic effects observed in the initial phase (2 h, 7 d), the delivery of Cu to the CSF and to the brain parenchyma is hampered. Recovery or overcompensation in the periventricular zones may be faster (as early as d 28) than in the parenchyma (later than d 28) due to the higher proliferative capacity of the ependyma. The endothelial transition compartment where Cu should be entrapped in this scenario is too small to be resolved by LA-ICP-MS or to measurably influence local averages. This interpretation is corroborated by histochemical studies localizing abundant ATP7A and ATP7B in periventricular regions and the fascia dentata [36, 38, 39]—the endothelium of small capillaries exclusively expressing ATP7B— and studies of Cu turnover using [^{67}Cu] applied in vivo and autoradiography. These showed a pattern congruent to the distribution of total Cu with by far the highest Cu uptake in periventricular zones and the fascia dentata [40].

In this context, effects observed in the mouse MPTP model may be noteworthy. Systemically administered inorganic Cu [41] was protective. The copper ionophore clioquinol (Figure 1) that increased cerebral Cu availability was protective [42]. The moderately lipophilic and less selective copper chelator diethyldithiocarbamate (Figure 1), which is assumed to decrease cerebral Cu availability and to inhibit superoxide dismutase was deleterious [43]. It seems likely that in parallel to the increase in NADH/NAD$^+$, MPTP causes an increase of Cu^+/Cu^{2+}, resulting in a mobilization of Cu from the bound to the free compartment.

In humans, increased CSF copper levels in PD patients [44], have been reported, but are not directly in

line with the findings on MPTP mice. However, clioquinol (Scheme 1) alleviated Alzheimer's disease [45].

The Fe increase in the interpeduncular nucleus and hypothalamic areas exemplifies the anatomic differences of the rodent MPTP model and the primate situation. MPTP action results from two prerequisites, the presence of MPTP binding sites, virtually on glial cells, and the expression of dopamine transporters on neurons that take up the toxic pyridinium metabolite MPP^+ [46, 47]. Receptor binding studies using [^{3}H]MPTP and autoradiography on brain slices revealed strong binding in the substantia nigra of humans, but only modest binding in mice, and low binding in rats. Coincidentally, primates are very sensitive to MPTP, mice less sensitive, and rats largely resistant. In mice, the hypothalamus and the periaqueductal gray were reported to be the regions with highest [^{3}H]MPTP binding, followed by the nucleus accumbens and the olfactory tubercle. The interpeduncular nucleus was not shown [46]. In rats, the highest binding was observed in the interpeduncular nucleus, locus coeruleus, arcuate and periventricular hypothalamic nuclei, the subfornical organ, and ventricular ependyma [48]. The situation in mice may be elucidated in more detail by studies of the distribution of monoamine oxidase (MAO-B), which is assumed to be identical with the [^{3}H]MPTP binding sites [46–48]. MAO-B, detected by receptor autoradiography, was found to be most abundant in mouse raphe nuclei, paraventricular thalamic nuclei, ependyma, choroids plexus, periaqueductal gray, and in the interpeduncular nucleus [49]. Indeed, findings obtained by us (unpublished) and others point to some dopaminergic innervation of the interpeduncular nucleus, a complex and highly differentiated structure where cholinergic afferents and glutamatergic output seem to predominate [50, 51]. Amongst possible causes of regional Fe increase after MPTP, an increased expression of divalent metal transporter 1 isoform IRE+ transporting non-transferrin-bound Fe^{2+} was observed on dopaminergic neurons and activated microglia [33]. The question is, which are the initial noxious events and which the secondary compensatory processes.

Conclusions

LA-ICP-MS imaging proved to be a valuable tool in preclinical research, yielding consistent and statistically significant results while analyzing treatment effects in a larger set of samples. LA-ICP-MS imaging has meanwhile reached routine scale. A global mapping of spatial analyte distribution guiding the targeted sampling of biological material may be advantageous in many cases. Findings and effects in small substructures may be diluted if larger structures are studied by dissection and bulk analysis. Here, micro-local analysis identified substructures of interest (periventricular zone, interpeduncular nucleus) and revealed that the structures of interest dissected in previous studies (striatum, mesencephalon) were chosen inappropriately. Our findings contribute an incentive for further pursuing the metallomic approach in research of and drug development for neurodegenerative diseases.

Acknowledgments

The authors thank A. Zimmermann (Forschungszentrum Jülich) for technical support with LA-ICP-MS measurements. This study was supported in part by the German Parkinson's Society and the University Hospitals of Gießen and Marburg, Germany.

References

1. Sigel, A.; Sigel, H.; Sigel, R. K.; Eds. *Neurodegenerative Diseases and Metal Ions*; John Wiley and Sons: Chichester, 2006; pp 1–435.
2. Qureshi, G. A.; Syed, S. A.; Parvez, S. H. Role of Selenium, Iron, Copper, and Zinc. In *Oxidative Stress and Neurodegenerative Disorders*; Qureshi, G. A.; Parvez, S. H., Eds. Elsevier: 2007; 719.
3. Hutchinson, R. W.; Cox, A. G.; McLeod, C. W.; Marshall, P. S.; Harper, A.; Dawson, E. L.; Howlett, D. R. Imaging and Spatial Distribution of β-Amyloid Peptide and Metal Ions in Alzheimer's Plaques by Laser Ablation-Inductively Coupled Plasma-Mass Spectrometry. *Anal. Biochem.* **2005,** *346*, 225–233.
4. Faucheux, B. A.; Martin, M. E.; Beaumont, C.; Hauw, J. J.; Agid, Y.; Hirsch, E. C. Neuromelanin Associated Redox-Active Iron Is Increased in the Substantia Nigra of Patients with Parkinson's Disease. *J. Neurochem.* **2003,** *86*, 1142–1148.
5. Berg, D.; Youdim, M. B.; Riederer, P. Redox Imbalance. *Cell Tissue Res.* **2004,** *318*, 201–213.
6. Olanow, C. W.; Good, P. F.; Shinotoh, H.; Hewitt, K. A.; Vingerhoets, F.; Snow, B. J.; Beal, M. F.; Calne, D. B.; Perl, D. P. Manganese Intoxication in the Rhesus Monkey: A Clinical Imaging, Pathologic, and Biochemical study. *Neurology* **1996,** *46*, 492–498.
7. Hill, J. M.; Switzer, R. C. III. The Regional Distribution and Cellular Localization of Iron in the Rat Brain. *Neuroscience* **1984,** *11*, 595–603.
8. Popescu, B.; George, M.; Bergmann, U.; Garachtchenko, A.; Kelly, M.; McCrea, R.; Lüning, K.; Devon, R.; George, G.; Hanson, A.; Harder, S.; Chapman, L.; Pickering, I.; Nichol, H. Mapping Metals in Parkinson's and Normal Brain Using Rapid-Scanning X-ray Fluorescence. *Phys. Med. Biol.* **2009,** *54*, 651–663.
9. Chwiej, J.; Fik-Mazgaj, K.; Szczerbowska-Boruchowska, M.; Lankosz, M.; Ostachowicz, J.; Adamek, D.; Simionovici, A.; Bohic, S. Classification of Nerve Cells from Substantia Nigra of Patients with Parkinson's Disease and Amyotrophic Lateral Sclerosis with the Use of X-ray Fluorescence Microscopy and Multivariate Methods. *Anal. Chem.* **2005,** *77*, 2895–2900.
10. Ektessabi, A.; Yoshida, S.; Takada, K. Distribution of Iron in a Single Neuron of Patients with Parkinson's Disease. *X-Ray Spectrom.* **1999,** *28*, 456–460.
11. Becker, J. S. *Inorganic Mass Spectrometry: Principles and Applications*; John Wiley and Sons: Chichester, 2007; pp 317–380.
12. Becker, J. S.; Zoriy, M. V.; Pickhardt, C.; Palomero-Gallagher, N.; Zilles, K. Imaging of Copper, Zinc, and Other Elements in Thin Section of Human Brain Samples (Hippocampus) by Laser Ablation Inductively Coupled Plasma Mass Spectrometry. *Anal. Chem.* **2005,** *77*, 3208–3216.
13. Becker, J. S.; Zoriy, M. V.; Dehnhardt, M.; Pickhardt, C.; Zilles, K. Copper, Zinc, Phosphorus, and Sulfur Distribution in Thin Section of Rat Brain Tissues Measured by Laser Ablation Inductively Coupled Plasma Mass Spectrometry: Possibility for Small-Size Tumor Analysis. *J. Anal. Atom. Spectrom.* **2005,** *20*, 912–917.
14. Becker, J. S.; Zoriy, M.; Pickhardt, C.; Damoc, E.; Juhacz, G.; Palkovits, M.; Przybylski, M. Determination of Phosphorus-, Copper-, and Zinc-Containing Human Brain Proteins by LA-ICPMS and MALDI-FTICR-MS. *Anal. Chem.* **2005,** *77*, 5851–5860.
15. Becker, J.; Matusch, A.; Depboylu, C.; Dobrowolska, J.; Zoriy, M. Quantitative Imaging of Selenium, Copper, and Zinc in Thin Sections of Biological Tissue (Slugs–Genus Arion) Measured by LA-ICP-MS. *Anal. Chem.* **2007,** *79*, 6074–6080.
16. Dobrowolska, J.; Dehnhardt, M.; Matusch, A.; Zoriy, M.; Palomero-Gallagher, N.; Koscielniak, P.; Zilles, K.; Becker, J. S. Quantitative Imaging of Zinc, Copper, and Lead in Three Distinct Regions of the Human Brain by Laser Ablation Inductively Coupled Plasma Mass Spectrometry. *Talanta* **2008,** *74*, 717–723.
17. Zoriy, M.; Matusch, A.; Spruss, T.; Becker, J. S. Laser Ablation Inductively Coupled Plasma Mass Spectrometry for Imaging of Copper, Zinc, and Platinum in Thin Sections of a Kidney from a Mouse Treated with cis-Platin. *Int. J. Mass Spectrom. Mass Spectrom.* **2007,** *260*(Special Issue), 102–106.
18. Zoriy, M. V.; Dehnhardt, M.; Reifenberger, G.; Zilles, K.; Becker, J. S. Imaging of Cu, Zn, Pb, and U in Human Brain Tumor Resections by Laser Ablation Inductively Coupled Plasma Mass Spectrometry. *Int. J. Mass Spectrom.* **2006,** *257*, 27–33.
19. Pozebon, D.; Dressler, V.; Matusch, A.; Becker, J. Monitoring of Platinum in a Single Hair by Laser Ablation Inductively Coupled Plasma

Mass Spectrometry (LA-ICP-MS) After Cisplatin Treatment of Cancer. *Int. J. Mass Spectrom.* **2008,** *272*, 57–62.
20. Becker, J. S.; Pozebon, D.; Dressler, V. L.; Lobinski, R.; Becker, J. S. LA-ICP-MS Studies of Zinc Exchange by Copper in Bovine Serum Albumin Using an Isotopic Enriched Copper Tracer. *J. Anal. At. Spectrom.* **2008,** *23*, 1076–1082.
21. Zoriy, M.; Dehnhardt, M.; Matusch, A; Becker, J. S. Comparative Imaging of P, S, Fe, Cu, Zn, and C in Thin Sections of Rat Brain Tumor as well as Control Tissues by Laser Ablation Inductively Coupled Plasma Mass Spectrometry. *Spectrochim. Acta B* **2008,** *63*, 375–382.
22. Becker, J. S.; Zoriy, M.; Matusch, A.; Salber, D.; Palm, C.; Becker, J. S. Bioimaging of Metals by Laser Ablation Inductively Coupled Plasma Mass Spectrometry (LA-ICP-MS). *Mass Spectrom. Rev.* **2009**, published on-line, DOI 10.1002/mas. 20239.
23. Becker, J. S.; Zoriy, M.; Wu, B.; Matusch, A.; Becker, J. Su. Imaging of Essential and Toxic Elements in Biological Tissues by LA-ICP-MS. *J. Anal. At. Spectrom.* **2008,** *23*, 1275–1280.
24. Pickhardt, C.; Izmer, A.; Zoriy, M.; Schaumloffel, D.; Becker, J. S. On-Line Isotope Dilution in Laser Ablation Inductively Coupled Plasma Mass Spectrometry Using a Microflow Nebulizer Inserted in the Laser Ablation Chamber. *Int. J. Mass Spectrom.* **2006,** *248*, 136–141.
25. Markey, S.; Johannessen, J.; Chiueh, C.; Burns, R.; Herkenham, M. Intraneuronal Generation of a Pyridinium Metabolite May Cause Drug-Induced Parkinsonism. *Nature* **1984,** *311*, 464–467.
26. Shimoji, M.; Zhang, L.; Mandir, A. S.; Dawson, V. L.; Dawson, T. M. Absence of Inclusion Body Formation in the MPTP Mouse Model of Parkinson's Disease. *Brain Res. Mol. Brain Res.* **2005,** *134*, 103–108.
27. Jackson-Lewis, V.; Przedborski, S. Protocol for the MPTP Mouse Model of Parkinson's Disease. *Nat. Protoc.* **2007,** *2*, 141–151.
28. Hare, D.; Reedy, B.; Grimm, R.; Wilkins, S.; Volitakis, I.; George, J.; Cherny, R.; Bush, A.; Finkelstein, D.; Doble, P. Quantitative Elemental Bioimaging of Mn, Fe, Cu, and Zn in 6-Hydroxydopamine Induced Parkinsonism Mouse Models. *Metallomics* **2009,** *1*, 53–58.
29. Paxinos, G.; Franklin, K. B. J. *The Mouse Brain in Stereotaxic Coordinates*, 2nd edition, Paxinos, G., Franklin, K. B. J., Eds.; Academic Press: San Diego, 2001.
30. Hoglinger, G. U.; Breunig, J. J.; Depboylu, C.; Rouaux, C.; Michel, P. P.; Alvarez-Fischer, D.; Boutillier, A. L.; Degregori, J.; Oertel, W. H.; Rakic, P.; Hirsch, E. C.; Hunot, S. The pRb/E2F Cell-Cycle Pathway Mediates Cell Death in Parkinson's Disease. *Proc. Natl. Acad. Sci. U.S.A.* **2007,** *104*, 3585–3590.
31. Weihe, E.; Depboylu, C.; Schutz, B.; Schafer, M. K.; Eiden, L. E. Three Types of Tyrosine Hydroxylase-Positive CNS Neurons Distinguished by Dopa Decarboxylase and VMAT2 Coexpression. *Cell. Mol. Neurobiol.* **2006,** *26*, 659–678.
32. Rios, C.; Alvarez-Vega, R.; Rojas, P. Depletion of Copper and Manganese in Brain after MPTP Treatment of Mice. *Pharmacol. Toxicol.* **1995,** *76*, 348–352.
33. Salazar, J.; Mena, N.; Hunot, S.; Prigent, A.; Alvarez-Fischer, D.; Arredondo, M.; Duyckaerts, C.; Sazdovitch, V.; Zhao, L.; Garrick, L. M.; Nunez, M. T.; Garrick, M. D.; Raisman-Vozari, R.; Hirsch, E. C. Divalent Metal Transporter 1 (DMT1) Contributes to Neurodegeneration in Animal Models of Parkinson's Disease. *Proc. Natl. Acad. Sci. U.S.A.* **2008,** *105*, 18578–18583.
34. Jiang, H.; Qian, Z. M.; Xie, J. X. [Increased DMT1 Expression and Iron Content in MPTP-Treated C57BL/6 Mice]. *Sheng Li Xue Bao* **2003,** *55*, 571–576.
35. Tarohda, T.; Ishida, Y.; Kawai, K.; Yamamoto, M.; Amano, R. Regional Distributions of Manganese, Iron, Copper, and Zinc in the Brains of 6-hHydroxydopamine-Induced Parkinsonian Rats. *Anal. Bioanal. Chem.* **2005,** *383*, 224–234.
36. Choi, B.; Zheng, W. Copper Transport to the Brain by the Blood-Brain Barrier and Blood-CSF Barrier. *Brain Res.* **2009,** *1248*, 14–21.
37. Lee, J.; Peña, M. M. ; Nose, Y.; Thiele, D. J. Biochemical Characterization of the Human Copper Transporter Ctr1. *J. Biol. Chem.* **2002,** *277*, 4380–4387.
38. Schlief, M. L.; Craig, A. M.; Gitlin, J. D. NMDA Receptor Activation Mediates Copper Homeostasis in Hippocampal Neurons. *J. Neurosci.* **2005,** *25*, 239–246.
39. Saito, T.; Okabe, M.; Hosokawa, T.; Kurasaki, M.; Hata, A.; Endo, F.; Nagano, K.; Matsuda, I.; Urakami, K.; Saito, K. Immunohistochemical Determination of the Wilson Copper-Transporting P-Yype ATPase in the Brain Tissues of the Rat. *Neurosci. Lett.* **1999,** *266*, 13–16.
40. Wang, L.; Wu, Q.; Becker, J.; Oliveira, M.; Bozza, F.; Schawager, A.; Lee, M.; Hoffman, J.; Morton, K. Decreased Copper Uptake in Brains of Aging Mice. **2009,** in press.
41. Rubio-Osornio, M.; Montes, S.; Perez-Severiano, F.; Aguilera, P.; Floriano-Sanchez, E.; Monroy-Noyola, A.; Rubio, C.; Rios, C. Copper Reduces Striatal Protein Nitration and Tyrosine Hydroxylase Inactivation Induced by MPP+ in Rats. *Neurochem. Int.* **2009,** *54*, 447–451.
42. Kaur, D.; Yantiri, F.; Rajagopalan, S.; Kumar, J.; Mo, J. Q.; Boonplueang, R.; Viswanath, V.; Jacobs, R.; Yang, L.; Beal, M. F.; DiMonte, D.; Volitaskis, I.; Ellerby, L.; Cherny, R. A.; Bush, A. I.; Andersen, J. K. Genetic or Pharmacologic Iron Chelation Prevents MPTP-Induced Neurotoxicity In Vivo: A Novel Therapy for Parkinson's Disease. *Neuron* **2003,** *37*, 899–909.
43. Corsini, G.; Pintus, S.; Chiueh, C.; Weiss, J.; Kopin, I. 1-Methyl-4-Phenyl-1,2,3,6-Tetrahydropyridine (MPTP) Neurotoxicity in Mice is Enhanced by Pretreatment with Diethyldithiocarbamate. *Eur. J. Pharmacol.* **1985,** *119*, 127–128.
44. Boll, M.; Alcazaz-Zubeldia, M.; Montes, S.; Rios, C. Free Copper, Ferro-Oxidase and SOD1 Activities, Lipid Peroxidation, and NO(x) Content in the CSF. A Different Marker Profile in Four Neurodegenerative Diseases. *Neurochem. Res.* **2008,** *33*, 1717–1723.
45. Treiber, C.; Simons, A.; Strauss, M.; Hafner, M.; Cappai, R.; Bayer, T. A.; Multhaup, G. Clioquinol Mediates Copper Uptake and Counteracts Copper Efflux Activities of the Amyloid Precursor Protein of Alzheimer's Disease. *J. Biol. Chem.* **2004,** *279*, 51958–51964.
46. Przedborski, S.; Kostić, V.; Jackson-Lewis, V.; Carlson, E.; Epstein, C. J.; Cadet, J. L. Quantitative Autoradiographic Distribution of [^{3}H]MPTP Binding in the Brain of Superoxide Dismutase Transgenic Mice. *Brain Res. Bull.* **1991,** *26*, 987–991.
47. Javitch, J. A.; D'Amato, R. J.; Strittmatter, S. M.; Snyder, S. H. Parkinsonism Inducing Neurotoxin, N-Methyl-4-Phenyl-1,2,3,6-Tetrahydropyridine: Uptake of the Metabolite N-Methyl-4-Phenylpyridinium by Dopamine Neurons Explain Selective Toxicity. *Proc. Natl. Acad. Sci. U.S.A.* **1985,** *82*, 2173–2177.
48. Javitch, J. A.; Uhl, G.; Snyder, S. Parkinson-Inducing Neurotoxin, N-methyl-4-Phenyl-1,2,3,6-Tetrahydropyridine: Characterization and Localization of Receptor Binding Sites in Rat and Human Brain. *Proc. Natl. Acad. Sci. U.S.A.* **1984,** *81*, 4591–4595.
49. Saura, J.; Richards, J. G.; Mahy, N. Differential Age-Related Changes of MAO-A and MAO-B in Mouse Brain and Peripheral Organs. *Neurobiol. Aging* **1994,** *15*, 399–408.
50. Gottesfeld, Z. Lesion-Induced Catecholaminergic Sprouting in the Interpeduncular Nucleus. *Neurochem. Res.* **1984,** *9*, 325–331.
51. Morley, B. J. The Interpeduncular Nucleus. *Int. Rev. Neurobiol.* **1986,** *28*, 157–182.